DOI: 10.1002/ejic.201000999

Solvothermal Synthesis, Characterization, and Formation Mechanism of a Single-Layer Anatase TiO_2 Nanosheet with a Porous Structure

Yajie Chen,[a] Guohui Tian,[a] Zhiyu Ren,[a] Chungui Tian,[a] Kai Pan,[a] Wei Zhou,[a] and Honggang Fu*[a]

Keywords: Titanium / Nanostructures / Solvothermal synthesis / Microporous materials / Raman spectroscopy

A novel single-layer polycrystalline anatase TiO_2 (SLP TiO_2) nanosheet with porous structure was synthesized through a simple solvothermal method by employing rod-like titanyl sulfate as the starting material in the presence of glycerol, followed by calcination. SEM, TEM, X-ray diffraction, FTIR spectroscopy, thermogravimetry coupled to FTIR spectroscopy, solid-state ^{13}C NMR spectroscopy, and N_2 adsorption/desorption processes were employed to investigate the structure of the products. The structure and morphology were found to be dependent on the experimental conditions, such as solvothermal reaction time, morphology of titanyl sulfate, and solvent type. The obtained SLP TiO_2 nanosheet was employed as a support for loading well-dispersed Ag nanoparticles and proved to be a good surface-enhanced Raman scattering (SERS) substrate for the detection of 4-aminothiophenol and Rhodamine 6G, showing great potential as a convenient and powerful substrate for SERS studies in the field of detecting different target molecules due to good uniformity and reliability.

Introduction

Recently, extensive attention has been focused on controlling the shape, size, morphology, distribution, and spatial arrangement of nanostructured materials because of the strong correlation between these parameters and their physical/chemical properties.[1–4] Meanwhile, increasing interest has been paid to the self-assembly of nanoscale building blocks into complex structures, because they can exhibit new and/or better properties.[5–9] As such, hierarchical nanostructured materials assembled in zero (nanoparticles, quantum dots), one (nanowires, nanorods, etc.), or two dimensions (nanoplates, nanosheets, etc.) have been recently investigated and found to show distinctive physicochemical properties in comparison with conventional nanocrystallites.

TiO_2 is one of the most important semiconductor materials for many applications, such as photocatalysis, environmental pollution control, solar energy conversion, gas sensing, and surface-enhanced Raman scattering (SERS).[10–13] To date, much effort has been directed to fabricate TiO_2 nanomaterials with special structures and morphologies, such as nanotubes, nanosheets, hollow spheres, nanorods, and nanowires, which have attracted great interest due to their excellent catalytic, electronic, optical, and mechanical properties.[14–19] Among these nanostructures, nanosheets have received wide attention in recent years and have been reported by many groups.[20,21] Most of the reported TiO_2 nanosheets have been prepared through an alkaline hydrothermal process by using TiO_2 powder as precursor, or prepared from protonic titanate hydrates by either calcination or hydro/solvothermal reactions, and show a single-crystalline structure.[22,23] There are, however, only very few reports[20] on the fabrication of two-dimensional polycrystalline TiO_2 nanosheets with porous and high-surface areas arising from the assembly of nanoparticles as the building blocks; these structures are potentially useful as catalysts and may act as SERS substrate and active components in fabricating gas sensors.

In this paper, we report the preparation of a single-layer polycrystalline anatase TiO_2 (SLP TiO_2) nanosheet with a porous structure through a simple solvothermal method by employing, as the starting material, rod-like titanyl sulfates in the presence of glycerol, followed by a calcination process. The possible formation mechanism was proposed based on our experimental results. The obtained TiO_2 nanosheets possess a polycrystalline and highly porous net-like structure made of interconnected nanoparticles. Polycrystalline sheets are assemblies of nanoparticles, which are very different from the previously reported single-crystalline TiO_2 nanosheets formed on the basis of the normal concept for crystal growth. The nanosheet was then modified with well-dispersed Ag nanoparticles to give an SERS substrate used to study the SERS activity by using 4-aminothiophenol (4-ATP) and Rhodamine 6G (Rh 6G) as molecular

[a] Key Laboratory of Functional Inorganic Material Chemistry, Heilongjiang University, Ministry of Education of the People's Republic of China,
Harbin 150080, P. R. China
Fax: +86-451-8667-3647
E-mail: fuhg@vip.sina.com

Supporting information for this article is available on the WWW under http://dx.doi.org/10.1002/ejic.201000999.

probes. It was found that the as-synthesized polycrystalline anatase Ag/TiO_2 nanosheet composites exhibited high SERS activity, overall good uniformity, and reliability.

Results and Discussion

Structure and Morphology of the Precursor and TiO_2 Nanosheet

Figure 1A shows the XRD patterns of the precursor material for the different solvothermal reaction times. For reference, the XRD pattern of the $TiOSO_4{\cdot}2H_2O$ starting material is also shown [curve (e)]. There are obvious differences in the XRD patterns between $TiOSO_4{\cdot}2H_2O$ and other precursor materials. The XRD pattern of $TiOSO_4{\cdot}2H_2O$ shows two strong peaks at 11 and 18°. These peaks, however, did not appear in the XRD patterns of the precursor materials after the solvothermal reaction. The XRD patterns of the precursor materials obtained from different solvothermal times exist as one sharp peak at about 7° with several weak peaks at relatively higher 2θ angles, which is characteristic of metal glycerolate.[24,25] Therefore, it could be concluded that, in the reaction system, glycerol served as a chelating ligand and coordinated in situ with $TiOSO_4$ to form the titanium glycerolate (TiGly) precursor complexes (Figure S1), which is similar to previous reports.[26,27] After we calcined the precursors at 600 °C in air for 3 h, the XRD diffraction peaks of the as-obtained products (Figure 1B) were in good agreement with pure anatase TiO_2 (JCPDS 21-1272), revealing the phase transformation from TiGly to anatase TiO_2. Meanwhile, $TiOSO_4{\cdot}2H_2O$ can also directly convert to anatase TiO_2 after calcination [see curve (e) in Figure 1B], which is consistent with a previous report.[28] Nevertheless, there is a great difference between the calcined products of $TiOSO_4{\cdot}2H_2O$ and TiGly on morphologies, which can be seen from the SEM images shown in Figure 3 (and Figure S2 in the Supporting Information).

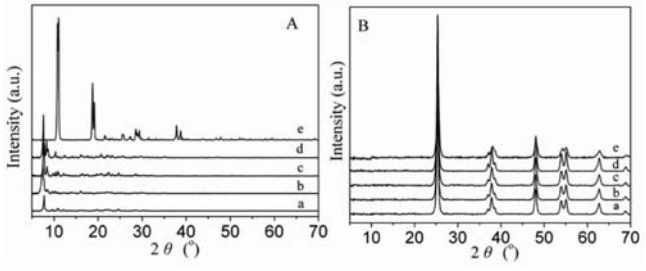

Figure 1. XRD patterns of commercial rod-like $TiOSO_4{\cdot}2H_2O$ (e) and titanium glycerolate precursors obtained from different solvothermal reaction times [(a) 1, (b) 6, (c) 12, (d) 24 h] before calcination (A) and the corresponding products after calcination (B).

Figure 2A shows the SEM and TEM (inset) images of the titanyl sulfate ($TiOSO_4{\cdot}2H_2O$) starting material, which exhibits a rod-like morphology with smooth surfaces. The rod-like $TiOSO_4{\cdot}2H_2O$ is 1–3 μm in diameter and 10–30 μm in length. Figure 2B–F show the FESEM images of the precursor obtained at different stages of the solvothermal reaction process, clearly reflecting the evolution process of the precursor morphology. The structure and morphology of the precursors were found to be largely dependent on the solvothermal reaction time. As shown in Figure 2B, the resulting white precursor obtained from a 0.5 h reaction time is a rod with an arris-structured edge; the rods are longer than 10 μm with diameters in the range of 0.8–3 μm. On increasing the reaction time to 1 h, the rods unfolded, and the nanosheets making up the rods become loosely packed (Figure 2C). Interestingly, thick nanosheets can be formed at the expense of nanorods on further increasing the reaction time. On increasing the reaction time to 6 h, only thick nanosheets exist in the reaction product, which are about 200–500 nm in thickness and 300–600 nm in width, but with no obvious change in length (above 10 μm). Moreover, the rod-like precursor disappeared completely. Such results could be observed from the SEM images in Figure 1D–E. Meanwhile, it could be found that the thick nanosheets gradually became thin on prolonging the reaction time because of splitting (Figure 2D–E). Eventually, single-layer nanosheets were produced as shown in Figure 2F; the nanosheets are relatively uniform and have a width of about 300–600 nm, a thickness of 30 nm, and a length of 5–10 μm.

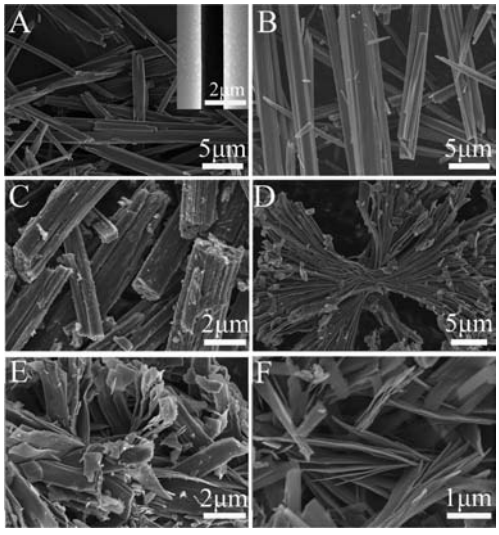

Figure 2. SEM and TEM (inset) images of the rod-like $TiOSO_4{\cdot}2H_2O$ starting material (A), and SEM images of the titanium glycerolate precursors prepared from different solvothermal reaction times: (B) 0.5, (C) 1, (D) 6, (E) 12, (F) 24 h.

After the synthesis of the TiGly precursors, the effect of the calcination on the morphologies of the products was investigated. Figures 3 and S2 show the SEM images of the calcined products, implying that they can easily transform to TiO_2 without major changes in the morphology and dimensions during the calcination process due to the existence of plenteous O atoms in the precursor.[24] Careful examination of many single-layer nanosheets reveals that the widths are mostly in the range of 300–500 nm; the thicknesses of the nanosheets can be deduced from the sheet, imaged edge-on, to be about 20–30 nm, which is just about the particle

size of a TiO_2 nanoparticle (Figure 3E–F). However, further observation of high-magnification SEM images (Figure 4A–B) of the side and top view of the TiO_2 nanosheets and the TEM image (Figure 4C) demonstrated that the nanosheet had been transformed from a dense structure with a relatively smooth surface into a highly porous sheet-like structure containing a large amount of interconnected nanoparticles with sizes of approximately 20 nm. The inserted selected-area electron-diffraction pattern (SAED) image in Figure 4C further proves the polycrystalline nature of the nanosheets. The corresponding high-resolution TEM (HRTEM) image in Figure 4D shows the fringe spacing of 0.35 nm corresponds well to that of crystallographic plane of anatase (101), which is consistent with previous results.[29,30]

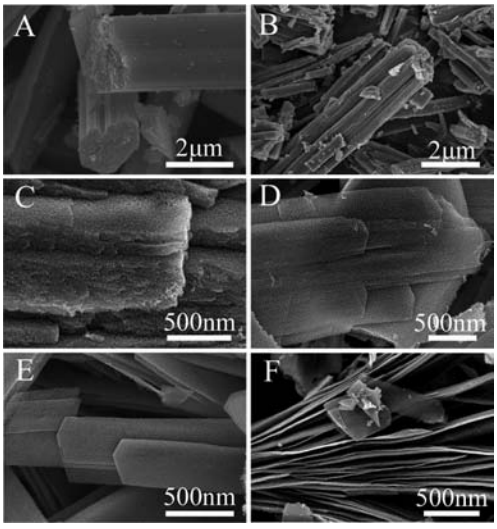

Figure 3. SEM images of the products obtained from the calcined precursor with different solvothermal reaction times: (A) 0.5, (B) 1, (C) 6, (D) 12, (E–F) 24 h.

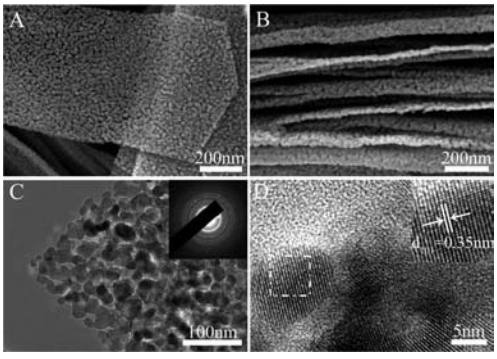

Figure 4. High-magnification SEM (A, B), TEM (C), and high-resolution TEM (HRTEM) (D) images of TiO_2 nanosheets obtained from the calcined precursor with a 24 h solvothermal reaction time. The inset of (C) shows the SAED patterns of the as-obtained TiO_2 nanosheet.

To study the structural changes of the precursor before and after calcination, infrared spectra were recorded and are shown in Figure 5. Curve (a) is the reference IR spectrum of glycerol. For the precursor and glycerol, the bands at 3436 and 1628 cm^{-1} correspond to the O–H stretching and the O–H bending modes, respectively, of both glycerol and traces of physically adsorbed water. The strong absorption bands lying in the 2500–3000 cm^{-1} domain are characteristics of the C–H stretching mode. Except for similar bands located below 2000 cm^{-1} due to C–C, C–O, and CH_2 bonds in the TiGly, a new IR absorption appears at 714 cm^{-1} for the as-prepared precursor, which is ascribed to the Ti–OH vibration similar to In–OH vibrations [curve (b)].[24] In addition, the band at 1059 cm^{-1} corresponding to the C–O stretching vibration shifts approximately 16 cm^{-1} to higher wavenumbers compared with the IR absorptions of pure glycerol, indicating the coordinating of C–O to metal cations.[31] After the TiGly was calcined at 600 °C in air for 3 h, the IR band at 400–850 cm^{-1} corresponds to the Ti–O–Ti stretching vibration mode in crystalline TiO_2; the occurrence of moderate peaks at 3436 and 1628 cm^{-1} explains the presence of adsorbed water [curve (c)].[32]

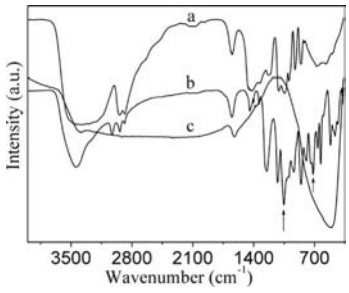

Figure 5. FTIR spectra of pure glycerol (a), the precursor (b), and the TiO_2 nanosheet (c).

Meanwhile, TG-FTIR-coupled simultaneous technique was used to analyze the gas product during thermal decomposition, together with the compositional and structural changes of the precursor. In Figure S3B in the Supporting Information, peaks in the regions of 665, 1372–1348, 1850–1450, 2300–2500, and 3900–3600 cm^{-1} were noted. The spectra fit well with the FTIR features of gas products of SO_2 (1372–1348 cm^{-1}), H_2O (1850–1450 and 3900–3600 cm^{-1}), and CO_2 (665 and 2300–2500 cm^{-1}) according to the standard IR spectra (Figure S4). The gravimetric temperature-programmed reaction curve is shown in Figure S3A. There are four major zones of mass loss in the TG curve, with a total mass loss of 67.0%. Together with the FTIR results of the evolved gas products in Figure S3B, the mass loss (4.2%) below 150 °C is ascribed to desorption of adsorbed water. The mass loss from 150 to 350 °C (32.2%) is attributed to the removal of glycerol units chemically bonded to Ti in the precursor. The mass loss (22.2%) from 350 to 450 °C arises from the dehydration of titanium oxyhydrate obtained from the reaction of $TiOSO_4$ with the trace water in the system (Figure S1) and the decomposition of small amounts of materials containing organic carbon. The fourth mass-loss step (8.4%) is the main decomposition process of sulfate ions above 530 °C, and the main evolution product at this step is sulfur dioxide (corresponding FTIR evolution peaks at 1372 and 1348 cm^{-1}). The decom-

position reactions corresponding to the thermal decomposition process of the precursor are shown in Figure S1.

Due to the insolubility of the TiGly powder in most of the organic solvents, ^{13}C NMR solid-state spectroscopy was carried out to gain some insight into the environment of the glycerol units, and the result is shown in Figure 6. Pure glycerol shows two peaks at δ = 62.1 and 71.6 ppm for the two end carbon atoms and the lone middle carbon atom, respectively (Figure 6B).[27] In the TiGly precursor, six distinguishable peaks are observed. The observed differences in the peak numbers and chemical shifts between the two samples suggest that the carbon atoms in the TiGly have significantly different local electronic environments compared with pure glycerol. Moreover, the difference of electronic environments among the carbon atoms in the TiGly was enough that six resolved peaks were detected. This is due to the fact that glycerol served as a chelating ligand and coordinated with Ti^{4+} to form sheet-like TiGly complexes. In this process, as a polyol, glycerol can participate in intramolecular reactions that reform alkoxytitanates and form nanosheet structures in the present system, leading to the complex carbon chemical environments.[33]

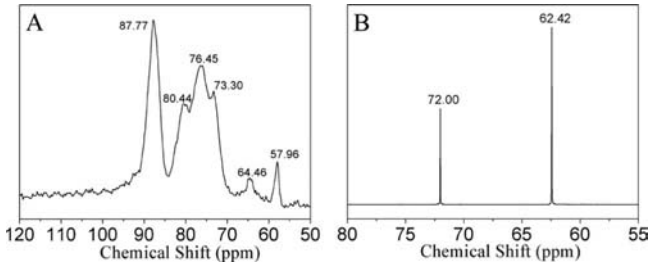

Figure 6. Solid-state CP/MAS ^{13}C NMR spectrum of the precursor prepared from the 24 h solvothermal reaction (A) and solution spectrum of pure glycerol (B).

N_2 adsorption/desorption isotherms (Figure 7) and the corresponding Barret–Joyner-Halenda (BJH) pore-size distribution plots (inset) of different TiO_2 nanosheet samples were performed to determine the surface area and pore structure. After calcination, the BET surface areas of the obtained TiO_2 nanosheets prepared under solvothermal reaction for 6, 12, and 24 h are 45, 50, and 56 $m^2 g^{-1}$, respectively. The slight increase of surface areas with increasing solvothermal reaction time can be attributed to the formation of thinner TiO_2 nanosheets, leading to a higher dispersion of the TiO_2 nanosheets. In addition, it is noteworthy that many pores with a diameter in the range of 10–50 nm appear in the TiO_2 nanosheets, which is attributed to the removal of organic species in the precursor. As a result, an interconnected net-like structure of TiO_2 nanoparticles form during calcination.

In this experiment, the morphology of the $TiOSO_4 \cdot 2H_2O$ starting material plays a key role to generate the rod-like and sheet-like precursors. To prove this assumption, a control experiment was performed by using crushed $TiOSO_4 \cdot 2H_2O$ as starting material. In this case, nanoparticles, not nanosheets, were observed from the SEM image (Figure S5), which indicated that the $TiOSO_4 \cdot 2H_2O$ starting

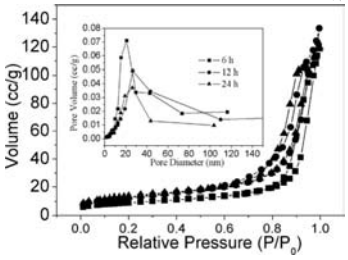

Figure 7. N_2 adsorption/desorption isotherm curves and pore-size distribution (inset) of the TiO_2 nanosheets obtained from the calcined precursors for different solvothermal reaction times (6, 12, 24 h).

material acted as both a self-sacrificing template and a slow-release titanium source in this reaction process. Meanwhile, DMSO, used as a "universal solvent", also plays an important role; glycerol thoroughly disperses throughout DMSO and therefore sufficiently reacts with rod-like solid $TiOSO_4$, thus leading to the dissolution of solid $TiOSO_4$ and the in situ synthesis of coordination complexes. The result of the control experiment without DMSO showed only large blocks (Figure S6), indicating that glycerol and solid $TiOSO_4$ could not interact and sufficiently react. In addition, the solvothermal reaction temperature also affects the formation of the single-layer nanosheet. When the solvothermal reaction was conducted at 110 °C for 24 h, keeping the other experimental conditions identical, only thick multi-layer TiO_2 nanosheets were formed (Figure S7); no single-layer nanosheets were found. Therefore, a proper reaction temperature should have a great influence on the production of single-layer nanosheets in the experiment, and the higher energy input provided by increasing the temperature may contribute to the splitting of thick multi-layer nanosheets.

Formation Mechanism

Based on the above experimental results, the possible formation mechanism of the SLP TiO_2 nanosheet with a porous structure is shown in Scheme 1. In our experiment, the rod-like morphology of the $TiOSO_4 \cdot 2H_2O$ starting material was crucial to achieve the sheet-like product, because it was used as both a self-sacrificing template and a titanium source. This can be confirmed by comparison with the experimental results from using the crushed rod-like $TiOSO_4 \cdot 2H_2O$ as starting material (Figure S5). Under solvothermal conditions, glycerol served as a chelating ligand and coordinated with Ti^{4+} to form TiGly complexes from the external part to the interior, which, in situ, aggregate into rods with arris-structured edges. With an increase in solvothermal reaction time, the rod-like precursor further breaks up into many thick nanosheets, indicating that a large rod-like precursor might consist of many thick nanosheets due to a weaker interaction (van der Waal forces) between layers relative to the stronger interaction between particles on each layer.[34,35] The formation of these thick nanosheets is believed to occur through a partial splitting of

exfoliated complex-precursor rods because of the impelling force of the solvent under solvothermal conditions. After a prolonged solvothermal reaction time (>12 h), the subsequent splitting of these intermediates caused the thick nanosheet to gradually become thin. Finally, a single-layer nanosheet was obtained, which can be observed from the SEM images (Figure 2E–F). To gain insight into the splitting process of thick nanosheets into single-layer nanosheets, we analyzed with GC/MS the nature of the liquid products separated from the solids. When the solvothermal time is 6 h, only DMSO and THF can be detected (Figure S8A). On further increasing the reaction time from 12 to 24 h, apart from these two matters, there are some other organics, the majority of which were identified as the products of the intermolecular condensation of DMSO (Figure S8B, C). In addition, there were also changes in the color of the liquid during the reaction process; the liquid is colorless within 12 h, as reaction proceeded, the color of the liquid gradually became dark brown. On keeping the solvothermal time (24 h) stationary and changing the solvothermal temperature to 110 °C, only the original materials of DMSO and THF could be detected (see Figure S8D); no additional materials were observed. All the above analyses indicate that long time, high pressure, and high temperature can promote reactions between organic solvent molecules and undermine the van der Waal forces between the layers, which contribute to the formation of single-layer nanosheets. Each formed TiGly single-layer nanosheet had a dense structure and a relatively smooth surface; calcination did not change the integral appearance of the sheet-like nanostructures due to the existence of plenteous O atoms in the precursor, as shown in Figure 4A–B. However, the removal of organic species in the precursor during calcination caused the formation of a porous structure in the TiO_2 nanosheet, which is made up of a large amount of interconnected nanoparticles.

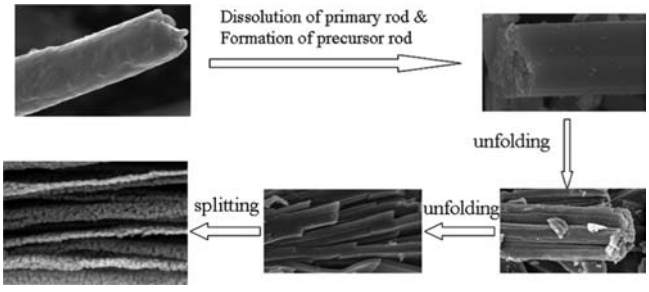

Scheme 1. Illustration of the formation process of the precursor nanosheet.

SERS Measurement

SERS is a power analytical tool for determining chemical information of molecules on solid substrates, and many metal-based substrates (such as Ag, Au, and Cu) have been widely used for SERS measurements.[36,37] Only a few semiconductor micro- or nanostructures are reported to produce low SERS signals,[38] such as TiO_2, which shows very weak SERS activity, thus limiting the breadth of practical applications for SERS in these metals relative to that in SERS-active metals.[39] It is therefore highly desirable to further improve the SERS activity on TiO_2. Studies showed that TiO_2 hybrid composites could contribute to enhance SERS activity compared to TiO_2.[40,41] There was, however, no report on the study of SERS activity on Ag/TiO_2 nanosheet composites.

To demonstrate the potential application, the as-prepared TiO_2 nanosheets were modified with well-dispersed Ag nanoparticles to explore the possibility to fabricate intense SERS substrates to detect different biological molecules. Compared with the normal Raman spectrum of solid 4-ATP (see Figure 8B), noticeable changes in the frequency shift and selective signal enhancement were observed for the SERS spectra of the Ag/TiO_2 nanosheet and Ag/TiO_2 nanoparticle composites (Figure 8D–E). The intensity of the bands located at 1140, 1389, 1438, and 1577 cm^{-1} (assigned to the b_2 vibration modes) and the band located at 1075 cm^{-1} (assigned to the a_1 vibration mode) of 4-ATP molecules were strongly enhanced. The increase in the b_2 vibration modes was attributed to the chemical mechanism, most likely from the charge transfer of the adsorbate to the metal, whereas the increase of the a_1 mode at 1075 cm^{-1} was due to an electromagnetic effect, which may be derived from the localized surface plasmon resonance of the Ag nanoparticles on the surface of the TiO_2 nanosheet.[42,43] Therefore, the SERS enhancement of our samples comes from both chemical and electromagnetic effects. It should be noticed that the Raman signals on the classical Lee–Meisel silver colloid and Ag/TiO_2 nanoparticle composites showed some decrease compared with that on the Ag/TiO_2 nanosheet composites. Moreover, the 4-ATP molecules did not exhibit any SERS activity from the unmodified TiO_2 nanosheet substrate (Figure 8A). The results showed that the prepared Ag/TiO_2 nanosheet composites should have a positive contribution to the enhancement of SERS activity. Each nanosheet is composed of highly porous net-like structure consisting of interconnected TiO_2 nanoparticles, and its surface was in close contact with the well-dispersed Ag nanoparticles according to the SEM image and EDX spectrum (Figure S9), which would increase the charge transfer between them under laser irradiation and contribute to the chemical effect of the whole SERS effects. Com-

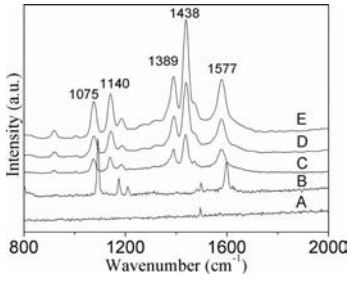

Figure 8. SERS spectra of 4-ATP on different substrates: TiO_2 nanosheet (line A), Raman spectrum of solid 4-ATP sample (line B), Lee's colloid (line C), Ag/TiO_2 nanoparticle composites (line D), and Ag/TiO_2 nanosheet composites (line E).

pared with the Ag/TiO_2 nanoparticle composites (the SEM image and EDX spectrum are shown in Figure S10), there is relatively uniform roughness and a high quantity of Ag nanoparticles exposed to the laser irradiation on the surface of TiO_2 nanosheet. Therefore, the obtained SERS substrate surfaces contain a great number of hot spots, which is favorable for enhancing the SERS signals.[37,44] Significantly, the SERS signals from the Ag/TiO_2 nanosheet composites showed less than 10% fluctuation over the entire substrate, indicating overall good uniformity and reliability of these substrate because of its relatively uniform roughness.

Rh 6G has been largely used for testing new SERS substrates. Thus, Rh 6G was chosen as another target molecule to evaluate the SERS activity on Ag/TiO_2 nanosheet composites. A good SERS signal was obtained for Rh 6G adsorbed onto an Ag/TiO_2 nanosheet composite compared with that of Rh 6G adsorbed on crushed Ag/TiO_2 nanoparticle composites, Ag colloids, and single TiO_2 nanosheet surfaces (Figure 9). The SERS signals observed at 1311, 1362, 1504, 1575, and 1650 cm^{-1} are attributed to the aromatic C–C stretching vibrations of the Rh 6G molecule, whereas the peak at 1184 cm^{-1} is associated with a C–C stretching vibration.[45,46] Therefore, our studies indicate that the present Ag/TiO_2 nanosheet composites are potential substrates for SERS studies in the field of detecting different target molecules.

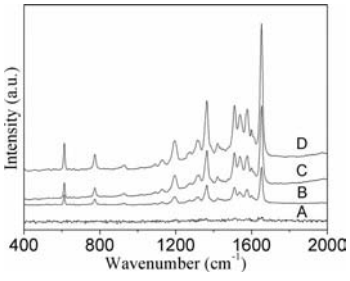

Figure 9. SERS spectra of Rh 6G on different substrates: TiO_2 nanosheet (line A), Lee's colloid (line B), Ag/TiO_2 nanoparticle composites (line C), and Ag/TiO_2 nanosheet composites (line D).

Conclusion

A simple solvothermal method was developed to synthesize a novel SLP TiO_2 nanosheet with a porous structure. The experimental conditions, such as solvothermal reaction time, morphology of titanyl sulfate, solvent type, and temperature, had a great influence on the formation of the SLP TiO_2 nanosheet. The possible formation mechanism was proposed based on our experimental results. The results showed that the as-obtained TiO_2 nanosheet modified with Ag could be used as a good SERS substrate for the detection of 4-ATP and Rh 6G, showing a great potential as a convenient and powerful SERS substrate for the detection of different biological molecules due to good uniformity and reliability. Moreover, such a porous SLP TiO_2 nanosheet has possible applications in other important fields, such as catalysis, gas sensing, and antibacterial science.

Experimental Section

Synthesis of SLP TiO_2 Nanosheets with Porous Structure: All the reactants were commercial and used without further purification. Rod-like solid $TiOSO_4{\cdot}2H_2O$ was purchased from Dandong Zhonghe Chemical plant (Dandong, China), and other chemicals were purchased from Shanghai Chemical Reagent Co. (Shanghai, China). For the preparation of SLP TiO_2 nanosheets with porous structure, a typical synthetic process was as follows: Glycerol (5 mL) was added to a mixture containing DMSO (20 mL) and THF (10 mL), and then $TiOSO_4{\cdot}2H_2O$ (0.5 g) was added with stirring. The as-formed suspension was added placed in a 50 mL autoclave and heated at 160 °C for a period of time (0.5, 1, 6, 12, and 24 h). After cooling to room temp., the resulting white precipitate was centrifuged, washed with ethanol to remove excess solvent, and dried at 80 °C for 3 h. The products were calcined from room temp. to 600 °C at a rate of 2 °C min^{-1} and equilibrated at 600 °C in air for 3 h. For a comparative study, the experiment with crushed rod-like $TiOSO_4{\cdot}2H_2O$ as starting material was also conducted in which the other experimental conditions were kept constant.

Preparation of Ag/TiO_2 Composites: The prepared TiO_2 product (100 mg) was modified by treatment with a protonic PEI aqueous solution (2.5 g L^{-1}, pH = 9.0) for 30 min to introduce positive charges onto the surface, followed by thorough washing with Milli-Q water (5×) and then suspended in Milli-Q water (80 mL) yielding a suspension of TiO_2 nanosheets (3.2 g L^{-1}). Afterwards, an aqueous solution of $AgNO_3$ (1 mL, 0.02 mol L^{-1}) and $NaBH_4$(6.5 mg) were added to the functionalized TiO_2 nanosheet solution with vigorous stirring, which produced TiO_2 nanosheets interspersed with well-separated silver particles on the surface. The colloidal solution was then heated to 80 °C, and an $AgNO_3$ solution (0.5 mL, 0.05 mol L^{-1}) was added under vigorous stirring, followed by the addition of sodium citrate (0.5 mL, 0.15 mol L^{-1}); the reaction lasted for about 10 min. After cooling to room temp., the resultant precipitates were centrifuged, washed with ethanol, and dried at 60 °C for 3 h. In addition, the Ag colloid used as reference was prepared according to Lee's method.[47]

Characterization: The products were characterized by TEM (JEOL-2100) at an accelerating voltage of 200 kV, SEM (Hitachi, S-4800), XRD (Rigaku D/max diffractometer, Cu-K_α radiation, λ = 0.15406 nm), and BET analysis (Micromeritics ASAP 2010). FTIR spectra of the precursors before and after calcination were recorded with a Perkin–Elmer Spectrum One FTIR spectrometer by using the KBr pellet method. The released gas analyses of the decomposition process of the precursors were carried out by coupling the FTIR spectrometer (Nicolet iS10) to TG (TA Q600) using a 2 mm internal diameter Teflon tube with a heating rate of 5 °C/min under a flow of air. To reduce the possibility of gases condensing along the transfer line, the temperature in the gas cell and transfer line were set to 230 °C. A GC/MS plot of the liquid product was performed with an Agilent 6890N/5973I. The solid-state ^{13}C CPMAS spectrum was recorded with a Bruker Avance 400 WB spectrometer equipped with a 4 mm standard-bore CPMAS probe head, in which the X channel was tuned to 100.62 MHz for ^{13}C and the other channel was tuned to 400.18 MHz. Raman spectra were obtained with a Jobin–Yvon HR 800 spectrometer. The 457.9 nm radiation from a 20 mW air-cooled argon ion laser was used as the exciting source. The laser power at the sample position was typically 400 μW with an average spot size of 1 μm in diameter. Data acquisition time was 30 s.

SERS Measurement: To record the Raman spectrum of 4-ATP and Rh 6G adsorbed on Ag/TiO_2 composites substrates, an aqueous solution of the Ag/TiO_2 composites (0.1 mL, 30 g L^{-1}) was dropped

onto the glass substrate and dried under ambient conditions. Ethanol solutions of 4-ATP or Rh 6G (20 μL, 1.0×10^{-5} mol L^{-1}) were dropped onto the glass slides containing the samples. After evaporation of the solvent, SERS spectra were recorded under ambient conditions.

Supporting Information (see footnote on the first page of this article): The reaction formulas of the reactions in solution and the decomposition process of the product; SEM images of calcined rod-like $TiOSO_4 \cdot 2H_2O$ and the products prepared by using crushed $TiOSO_4 \cdot 2H_2O$ as starting material, without the use of DMSO, and the product prepared from the solvothermal reaction at 110 °C for 24 h; TG-FTIR spectra of the product and its decomposed gases. GC/MS plot of liquid product obtained after different reaction times and possible organics detected in the liquid separated from the solvothermal reaction product; SEM images and EDX spectra of the TiO_2 nanosheets and nanoparticles modified with Ag nanoparticles.

Acknowledgments

We gratefully acknowledge the support of this research by the Key Program Projects of the National Natural Science Foundation of China (No. 21031001), the National Natural Science Foundation of China (No. 20971040, 21001042), the Cultivation Fund of the Key Scientific and Technical Innovation Project, Ministry of Education of China (No. 708029), the Scientific Research Fund of Heilongjiang Provincial Education Department (No. 11541283), the Excellent Youth of Common Universities of Heilongjiang Province of China (No. 1154G24), the Harbin Youth Foundation (2009RFQXG202), and the China Postdoctoral Science Foundation (20080440919).

[1] Y. G. Sun, Y. N. Xia, *Science* **2002**, *298*, 2176–2179.
[2] F. X. Zhang, X. Carrier, J.-M. Krafft, Y. Yoshimurac, J. Blanchard, *New J. Chem.* **2010**, *34*, 508–516.
[3] H. X. Li, Z. F. Bian, J. Zhu, D. Q. Zhang, G. S. Li, Y. N. Huo, H. Li, Y. F. Lu, *J. Am. Chem. Soc.* **2007**, *129*, 8406–8407.
[4] D. H. Taffa, M. Kathiresan, L. Walder, B. Seelandt, M. Wark, *Phys. Chem. Chem. Phys.* **2010**, *12*, 1473–1482.
[5] E. Hosono, S. Fujihara, H. Imai, I. Honma, I. Masaki, H. S. Zhou, *ACS Nano* **2007**, *1*, 273–278.
[6] I. Bita, J. K. W. Yang, Y. S. Jung, C. A. Ross, E. L. Thomas, K. K. Berggren, *Science* **2008**, *321*, 939–943.
[7] S.-i. Izumi, H. Shimakoshi, M. Abe, Y. Hisaeda, *Dalton Trans.* **2010**, *39*, 3302–3307.
[8] J. J. Cheng, A. M. Mayes, C. A. Ross, *Nat. Mater.* **2004**, *3*, 823–828.
[9] D. P. Sun, J. Z. Yang, X. Wang, *Nanoscale* **2010**, *2*, 287–292.
[10] Y. Park, S.-H. Lee, S. O. Kang, W. Choi, *Chem. Commun.* **2010**, 2477–2479.
[11] Z. Y. Liu, X. T. Zhang, S. Nisimoto, T. Murakami, A. Fujishima, *Environ. Sci. Technol.* **2008**, *42*, 8547–8551.
[12] D. H. Chen, F. Z. Huang, Y. B. Cheng, R. A. Caruso, *Adv. Mater.* **2009**, *21*, 1–5.
[13] D. Kannaiyan, E. Kim, N. Won, K. W. Kim, Y. H. Jang, M.-A. Cha, D. Y. Ryu, S. Kim, D. H. Kim, *J. Mater. Chem.* **2010**, *4*, 677–682.
[14] P. Wang, S. M. Zakeeruddin, J. E. Moser, M. K. Nazeeruddin, T. Sekiguchi, M. Gratzel, *Nat. Mater.* **2003**, *2*, 402–407.
[15] Z. Zhou, R. Shinar, A. J. Allison, J. Shinar, *Adv. Funct. Mater.* **2007**, *17*, 3530–3535.
[16] R. Buonsanti, E. Snoeck, C. Giannini, F. Gozzo, M. Hernandez, M. A. Garcia, R. Cingolani, P. D. Cozzoli, *Phys. Chem. Chem. Phys.* **2009**, *11*, 3680–3691.
[17] K. Wang, M. Wei, M. A. Morris, H. Zhou, J. D. Holmes, *Adv. Mater.* **2007**, *19*, 3016–3020.
[18] A. Armstrong, R. G. Armstrong, J. Canales, P. G. Bruce, *Angew. Chem. Int. Ed.* **2004**, *43*, 2286–2288.
[19] Z. Y. Liu, D. D. Sun, P. Guo, J. O. Leckie, *Chem. Eur. J.* **2007**, *13*, 1851–1855.
[20] Y. M. Wang, G. Du, J. H. Liu, D. Liu, S. B. Qin, N. Wang, C. G. Hu, X. T. Tao, J. Jiao, J. Y. Wang, Z. L. Wang, *Adv. Funct. Mater.* **2008**, *18*, 1131–1317.
[21] K. Fukuda, I. Nakai, C. Oishi, M. Nomura, M. Harada, Y. Ebina, T. Sasaki, *J. Phys. Chem. B* **2004**, *108*, 13088–13092.
[22] H. Y. Zhang, T. H. Ji, Y. F. Liu, J. W. Cai, *J. Phys. Chem. C* **2008**, *112*, 8604–8608.
[23] Z. Y. Yuan, J. F. Colomer, L. Su, *Chem. Phys. Lett.* **2002**, *363*, 362–366.
[24] C. Q. Wang, D. R. Chen, X. J. Jiao, *J. Phys. Chem. C* **2009**, *113*, 7714–7718.
[25] D. Larcher, R. Sudant, R. Patrice, J.-M. Tarascon, *Chem. Mater.* **2003**, *15*, 3543–3551.
[26] R. Rémiás, Á. Kukovecz, M. Darányi, G. Kozma, S. Varga, Z. Kónya, I. Kiricsi, *Eur. J. Inorg. Chem.* **2009**, 3622–3627.
[27] J. Das, D. Khushalani, *J. Phys. Chem. C* **2010**, *114*, 2544–2550.
[28] M. Johnsson, P. Pettersson, M. Nygren, *Thermochim. Acta* **1997**, *298*, 47–54.
[29] Y. N. Fang, Q. Z. Wu, M. B. Dickerson, Y. Cai, S. Shian, J. D. Berrigan, N. Poulsen, N. K. N. Kroger, K. H. Sandhage, *Chem. Mater.* **2009**, *21*, 5704–5710.
[30] J. M. Li, Y. X. Yu, Q. W. Chen, J. J. Li, D. S. Xu, *Cryst. Growth Des.* **2010**, *10*, 2111–2115.
[31] Y. Y. Xu, D. R. Chen, X. L. Jiao, K. Y. Xue, *J. Phys. Chem. C* **2007**, *111*, 16284–16289.
[32] L. Q. Jing, H. G. Fu, B. Q. Wang, D. J. Wang, B. F. Xin, S. D. Li, J. Z. Sun, *Appl. Catal. B* **2006**, *62*, 282–291.
[33] Y. Chen, Y. Y. Yi, J. Brennan, M. Brook, *Chem. Mater.* **2006**, *18*, 5326–5335.
[34] X. C. Jiang, Y. L. Wang, T. Herricks, Y. N. Xia, *J. Mater. Chem.* **2004**, *14*, 695–703.
[35] Y. L. Wang, X. C. Jiang, Y. N. Xia, *J. Am. Chem. Soc.* **2003**, *125*, 16176–16177.
[36] H. H. Wang, C. Y. Liu, S. B. Wu, N. W. Liu, C. Y. Peng, T. H. Chan, C. F. Hsu, J. K. Wang, Y. L. Wang, *Adv. Mater.* **2006**, *18*, 491–495.
[37] T. Wang, X. Hu, S. Dong, *Small* **2008**, *4*, 781–786.
[38] L. G. Quanliano, *J. Am. Chem. Soc.* **2004**, *126*, 7393–7398.
[39] C. P. Leon, L. Kador, B. Peng, M. Thelakkat, *J. Phys. Chem. B* **2006**, *110*, 8723–8730.
[40] W. Song, Y. X. Wang, B. Zhao, *J. Phys. Chem. C* **2007**, *111*, 12786–12791.
[41] A. Musumeci, D. Gosztola, T. Schiller, N. M. Dimitrijevic, V. Mujica, D. Marren, T. Rajh, *J. Am. Chem. Soc.* **2009**, *131*, 6040–6041.
[42] M. Osawa, N. Matsuda, K. Yoshi, I. Uchida, *J. Phys. Chem.* **1994**, *98*, 12702–12707.
[43] X. G. Hu, T. Wang, L. Wang, S. J. Guo, S. J. Dong, *Langmuir* **2007**, *23*, 6352–6357.
[44] K. Kneipp, H. Kneipp, L. Itzkan, R. Dasari, M. S. Feld, *Chem. Rev.* **1999**, *99*, 2957–2976.
[45] L. B. Luo, L. M. Chen, M. L. Zhang, Z. B. He, W. F. Zhang, G. D. Yuan, W. J. Zhang, S. T. Lee, *J. Phys. Chem. C* **2009**, *113*, 9191–9196.
[46] M. W. Shao, L. Lu, H. Wang, S. Wang, M. L. Zhang, D. D. D. Ma, S. T. Lee, *Chem. Commun.* **2008**, *20*, 2310–2312.
[47] P. C. Lee, D. Meisel, *J. Phys. Chem.* **1982**, *86*, 3391–3395.

Received: September 18, 2010
Published Online: December 29, 2010

